Hindawi Publishing Corporation
International Journal of Photoenergy
Volume 2014, Article ID 752967, 12 pages
http://dx.doi.org/10.1155/2014/752967

Research Article

Excellent Silicon Surface Passivation Achieved by Industrial Inductively Coupled Plasma Deposited Hydrogenated Intrinsic Amorphous Silicon Suboxide

Jia Ge,[1,2] Muzhi Tang,[1] Johnson Wong,[1] Zhenhao Zhang,[3] Torsten Dippell,[3] Manfred Doerr,[3] Oliver Hohn,[3] Marco Huber,[3] Peter Wohlfart,[3] Armin G. Aberle,[1] and Thomas Mueller[1]

[1] *Solar Energy Research Institute of Singapore, National University of Singapore, Singapore 117574*
[2] *NUS Graduate School for Integrative Sciences and Engineering, National University of Singapore, Singapore 117456*
[3] *Singulus Technologies AG, Hanauer Landstraße 103, 63796 Kahl Am Main, Germany*

Correspondence should be addressed to Jia Ge; gejia@nus.edu.sg

Received 28 March 2014; Accepted 11 May 2014; Published 1 June 2014

Academic Editor: Aung Ko Ko Kyaw

We present an alternative method of depositing a high-quality passivation film for heterojunction silicon wafer solar cells, in this paper. The deposition of hydrogenated intrinsic amorphous silicon suboxide is accomplished by decomposing hydrogen, silane, and carbon dioxide in an industrial remote inductively coupled plasma platform. Through the investigation on CO_2 partial pressure and process temperature, excellent surface passivation quality and optical properties are achieved. It is found that the hydrogen content in the film is much higher than what is commonly reported in intrinsic amorphous silicon due to oxygen incorporation. The observed slow depletion of hydrogen with increasing temperature greatly enhances its process window as well. The effective lifetime of symmetrically passivated samples under the optimal condition exceeds 4.7 ms on planar *n*-type Czochralski silicon wafers with a resistivity of 1 Ωcm, which is equivalent to an effective surface recombination velocity of less than 1.7 cms^{-1} and an implied open-circuit voltage (V_{oc}) of 741 mV. A comparison with several high quality passivation schemes for solar cells reveals that the developed inductively coupled plasma deposited films show excellent passivation quality. The excellent optical property and resistance to degradation make it an excellent substitute for industrial heterojunction silicon solar cell production.

1. Introduction

Heterojunction silicon wafer (HET) solar cells have achieved very high efficiencies of up to 24.7% on a large area (101.8 cm^2) [1]. Its high efficiency mainly stems from an extremely high open-circuit voltage (V_{oc}) of up to 750 mV thanks to the excellent surface passivation. Such a cell structure has attracted attention not only due to its high conversion efficiency, but also due to its low process temperature which avoids bowing when using thin wafers [2, 3]. The insertion of a high-quality hydrogenated intrinsic amorphous silicon (a-Si:H(i)) thin film between the emitter (or back surface field) and the bulk material is the key to such a high cell efficiency [4–7]. Therefore, optimization of this buffer layer is of utmost importance.

Plasma-enhanced chemical vapour deposition (PECVD) of a-Si:H(i) has been the key to the successful industrial implementation of this technology as a passivation scheme, since the early 1990s [5, 8, 9], mainly thanks to its low temperature process and good surface passivation quality [10]. However, it is also reported that the optimization for such a layer is difficult because of possible epitaxial growth and the need to balance plasma species during deposition [11–14].

PECVD hydrogenated intrinsic amorphous silicon suboxide (a-SiO_x:H(i)) thin films are emerging as an alternative

to replace a-Si:H(i) as passivation layer in HET solar cells. Its excellent passivation quality and optical property has been demonstrated by several groups in recent years [15–19]. Notably, Mueller et al. [16, 18, 20, 21] have shown a record of high passivation quality on highly doped wafers using direct capacitively coupled plasma (CCP). The optical loss reported was also much lower than that of a-Si:H(i), proving promising potential as a passivation layer. However, in order to achieve a state-of-the-art passivation level, the mentioned group has used very high plasma frequencies (70–110 MHz) and prolonged annealing processes, which can be difficult to implement in industrial production. Furthermore, direct CCP can introduce extra damage to wafer surface during deposition, thus limiting the film's passivation quality.

In this paper, we present an alternative method of depositing a-SiO_x:H(i) thin film using a remote inductively coupled plasma (ICP) source operating at conventional frequency (13.56 MHz). It is well known that very high density plasma can be produced in an ICP system with low and narrowly distributed particle energy compared to CCP [22–24], and the wafer surface is less influenced by plasma condition by keeping substrate from plasma in a remote system. Therefore, the passivation quality of a-SiO_x:H(i) can be further improved with reduced process time. In this preliminary study, the optimization of a-SiO_x:H(i) is carried out in terms of passivation quality on highly doped material. The influence of CO_2 partial pressure and process temperature on the passivation quality is investigated. Detailed analyses, such as quasi-steady-state photoconductance (QSSPC) measurements, spectroscopic ellipsometry (SE), time-of-flight (TOF) secondary ion mass spectroscopy (SIMS), and Fourier transform infrared (FTIR) spectroscopy, are conducted to understand the passivation quality, film thickness, composition, optical bandgap, and chemical bonding configuration. In the last section, comparison with other high-quality passivation schemes is made in order to demonstrate the excellent passivation and optical qualities with good stability against ambient environment of the ICP a-SiO_x:H(i) films.

2. Experimental Details

The a-SiO_x:H(i) thin films were fabricated by decomposing silane (SiH_4), hydrogen (H_2), and carbon dioxide (CO_2) in a remote ICP system, the SINGULAR-HET. It is a fully automatic ICPECVD system developed by Singulus Technologies in collaboration with SERIS for industrial HET solar cell processing. The system has one infrared (IR) heating station (PS1) for preheating and four other process stations (PS2–PS5) for deposition. It has two stations (PS2 and PS5) for topside deposition and two stations (PS3 and PS4) for bottom-side deposition. Double-side deposition is accomplished by using PS2 and PS3 without breaking the vacuum. The process temperature is adjusted by changing the heater power setting in PS1 as well as the stabilization heater in each process station. The temperature is monitored by pyrometers installed after each station. The pyrometers are calibrated to Si wafers and verified using in situ thermal couple readings in the temperature range of interest. The Si wafers are loaded into the system using an automated cassette wafer handling unit. The structure and process cycle of the SINGULAR-HET is illustrated in Figures 1(a) and 1(b).

Table 1: Plasma parameter variation used in this paper.

Plasma parameter	Value/range
Power	750 W
Deposition time	1–60 s
$[SiH_4]/[H_2]$	1
CO_2 partial pressure (χ_o)	0–22%
Temperature	50–400°C

In each process station, the ICP source is driven by a radiofrequency (RF, 13.56 MHz) generator through a matching box. The reactive gases (H_2 and CO_2) are fed through a gas shower into the area surrounded by an inductive coil, where the plasma is generated. The deposition precursor gas (SiH_4) is introduced through a distribution ring outside the inductive coil near the wafers. The decomposed species travel downwards for PS2/5 onto the wafer surface to form the film. The ICP source and process station design are shown in Figure 1(c).

The a-SiO_x:H(i) films were deposited onto both sides of planar 160 μm thick 156 mm wide Czochralski (Cz) wafers with crystal orientation of ⟨100⟩. The choice of the n-type 1 Ωcm Cz wafer as the bulk material is based on the applicability to real HET solar cell fabrication. The film thickness was about 20 nm, except for the results shown in Section 3.1. This symmetrical a-SiO_x:H(i)/c-Si/a-SiO_x:H(i) structure was used to monitor the passivation quality. The same films were also deposited onto one side of highly resistive Si wafers for FTIR analyses. Before deposition, all wafers underwent an alkaline based silicon etch and a standard RCA (Radio Cooperation of America) cleaning followed by a one-minute dip in 1% hydrofluoric (HF) acid solution to remove the chemical oxide. After rinse and drying, the wafers were loaded onto substrate carriers and transferred into the load lock. Plasma parameters used in this work are summarized in Table 1. It should be noted that equal flow rates for SiH_4 and H_2 were used throughout this investigation. CO_2 flow rate was monitored and shown in terms of partial pressure defined by

$$\chi_o = \frac{[CO_2]}{[CO_2] + [SiH_4]} \times 100\%, \quad (1)$$

where square brackets represent the corresponding gas flow rate in standard cubic centimetre per minute (sccm). Furthermore, the process temperature is reported using the pyrometer reading on the wafer surface after PS1.

The effective minority carrier lifetime (τ_{eff}) of the symmetrical samples was determined using the QSSPC method in appropriate modes [39]. The τ_{eff} reported are as-deposited values extracted at a minority carrier injection level of 10^{15} cm^{-3} and approximately two minutes after deposition. Thermal annealing was avoided in this study so that the process is industrially compatible. The thickness of the film was determined by fitting SE data (300–800 nm). The fitting model comprised an underlying SiO_2 layer with a fixed

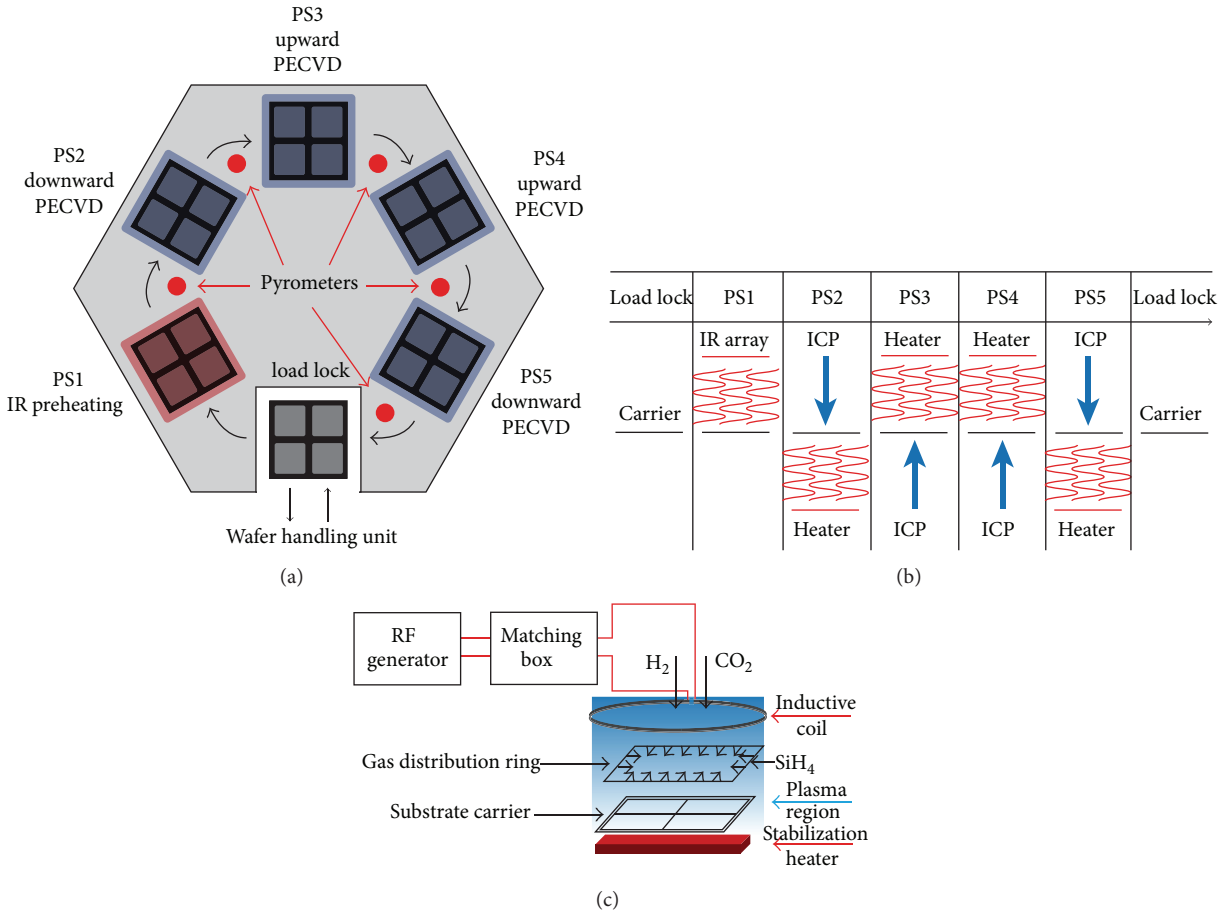

Figure 1: (a) Illustration of processing unit structure of the SINGULAR-HET. The arrows indicate the direction for carrier rotation and transfer. (b) Illustration of the process cycle. The horizontal arrow indicates processing order and the vertical arrows represent the direction of deposition in each station. (c) Illustration of process station and plasma design for plasma stations in downward deposition configuration. After [25, 26].

Table 2: Bonding types/modes and corresponding wavenumbers investigated by FTIR in this paper.

Bonding type	Mode wavenumber (cm^{-1})		
	Wagging/rocking	Bending	Stretching
Si–O–Si	—	810[a]	—
Si–H(Si_3)	640[b]	—	2000–2200[c]
Si–H(Si_2O)	—	—	1054[d,e]
Si–H(SiO_2)	—	—	1107[d,e]
Si–H(SiO_3)	—	—	1156[d,e]
$(SiH_2)_n$	—	845[f]	—
	—	883[f]	—

[a]Reference [34].
[b]Reference [35].
[c]Reference [36].
[d]Reference [15].
[e]Reference [37].
[f]Reference [38].

thickness of 1 nm, an a-SiO_x:H(i) layer characterized by Tauc-Lorentz (TL) model [40], and an overlayer consisting of 50% bulk material and 50% voids to represent the surface roughness. The absorption coefficient (α) of the film was determined from the fitted distinction coefficient (k) using $\alpha = 4\pi k/\lambda$, where λ is the wavelength.

The optical bandgap of the film was then determined by Tauc's method [41]. In order to investigate the bonding configuration in the film, FTIR measurement (500–4000 cm^{-1}) in transmission mode was carried out with a spectral resolution of 2 cm^{-1}. The bonding configurations of interest are summarized in Table 2. The total H content (C_H) in the film was obtained from the integrated intensity under the Si–H(Si_3) wagging mode peak [35], while the microstructure factor (r) was determined by the following equation [42]:

$$r = \frac{I_{2100}}{I_{2000} + I_{2100}}, \quad (2)$$

where I_j represents the integrated intensity under the peak denoted by the corresponding subscript. The peak intensity was obtained by deconvoluting the Si–H(Si_3) stretching peak using Gaussian curves. In particular, the peak centred at 2000 cm^{-1} usually represents monohydride configuration,

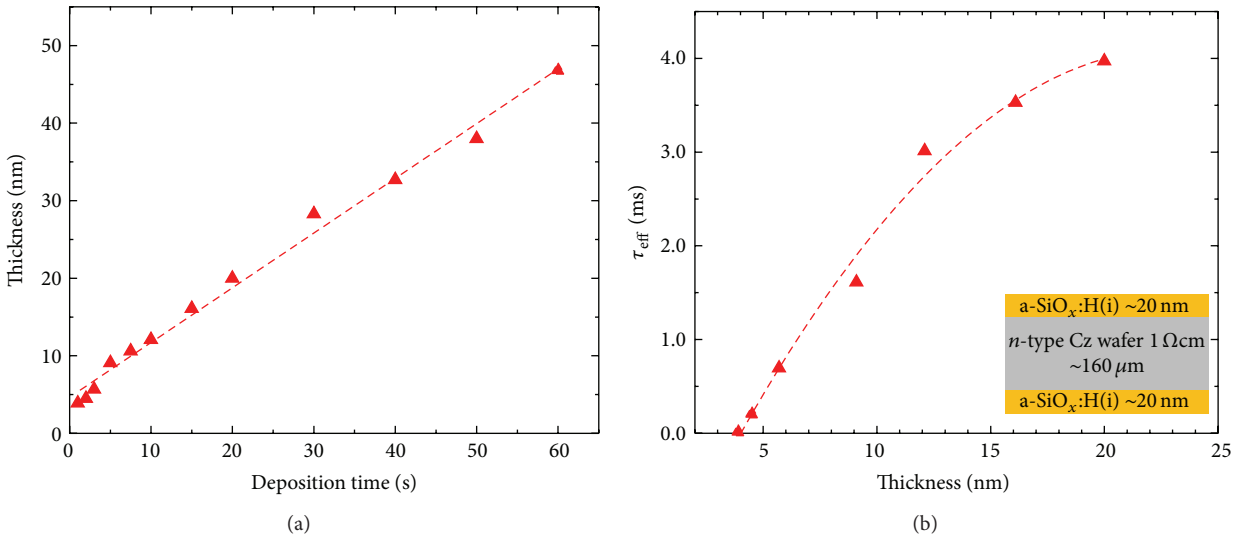

FIGURE 2: (a) a-SiO$_x$:H(i) thin film thickness as a function of deposition time; (b) τ_{eff} as a function of a-SiO$_x$:H(i) film thickness. The inset shows the sample structure used in lifetime determination. The lines are guides for the eye. A constant deposition rate is observed for all samples in this series. Lifetime saturation is observed after 20 nm film deposition.

while the peak at 2100 cm^{-1} represents the response from higher order hydrides [43, 44].

In order to quantify the atomic concentration of C and O under different χ_o, TOF SIMS (IONTOF) was conducted on selected samples using a 25 keV Bi+ beam with a current of 1 pA on a 80 × 80 μm^2 spot. Sputtering was done using a 1 keV Cs+ gun with a current of 8 nA on a 250 × 250 μm^2 area. The data were presented in both absolute atomic concentration per cubic centimetre and percentage over the host Si atoms. For percentage calculation, standard atomic concentration of crystalline Si was used (5×10^{22} cm^{-3}) without considering density change in amorphous material. This is justified by the negligible density change in amorphous Si reported by Smets et al. [45] and Remeš et al. [46, 47] under different C_H.

3. Results and Discussions

3.1. Deposition Time and Film Thickness. The investigation first focused on the deposition rate of a-SiO$_x$:H(i) in the ICP system in order to determine the thickness of film on which further optimization will be carried out. The result is shown in Figure 2(a).

A linear relationship between thickness and deposition time is observed, demonstrating a stable and robust deposition process for all samples. The nonzero interception at 0 deposition time can be attributed to the fluctuating plasma condition and nucleus formation at plasma ignition. A deposition rate of about 7 Å s^{-1} can be deduced from the slope of the linear fit. The same linear growth was also reported by Pysch et al. in a different ICP system for a-Si:H(i) deposition [48]. The linear behaviour can facilitate the thickness control in the subsequent optimization. Notably, the relatively high deposition rate can greatly reduce deposition time needed in real device fabrication. For a typical passivation layer of 5 nm or below, 1 to 2 s deposition is sufficient, thus largely enhancing the throughput.

The relationship between passivation quality and film thickness was then explored and presented in Figure 2(b). It can be observed that the passivation quality increases rapidly at low film thickness. The improvement of lifetime slows down after a film thickness of 10 nm and then tends to saturate after 20 nm. The saturation of τ_{eff} in terms of film thickness can be attributed to the reduction of interface defect density due to better network and surface coverage. This saturation effect was reported in the literature on different passivation materials [16, 24]. Further increase in film thickness can only provide marginal improvement of passivation quality, with the possible risk of inducing morphological change in the film (discussed in Section 3.3.3). Therefore, the film thickness is controlled at about 20 nm in this paper to ensure lifetime saturation. Such a thickness avoids second order effects that distort the actual passivation quality of the film while maintaining the minimal process time. At the same time, the similar film thickness ensures fair comparison on passivation quality across different plasma settings.

3.2. CO_2 Partial Pressure

3.2.1. Passivation Quality. While fixing the film thickness at about 20 nm, a scan on CO_2 partial pressure was performed in this experiment. Other plasma parameters were kept constant in this section. By varying the concentration of CO_2 in the plasma, compositional change that affected film passivation quality was expected. The lifetime results are illustrated in Figure 3.

It is shown that the increase of CO_2 partial pressure of up to about 10% improves passivation quality. Any increase beyond the optimal amount deteriorates the lifetime. The relatively low lifetime in Figure 3 is due to nonoptimized

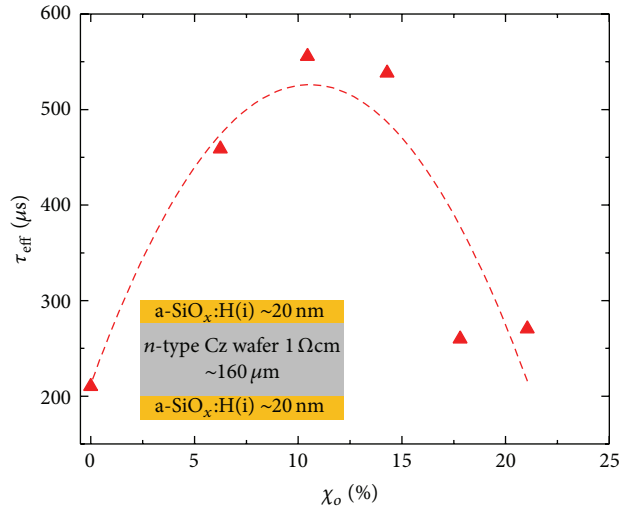

FIGURE 3: Lifetime as a function of CO_2 partial pressure while keeping other deposition conditions constant. The inset shows sample structure used in measuring lifetime. The line is a guide to the eye. A lifetime peak is observed at CO_2 partial pressure of 10%.

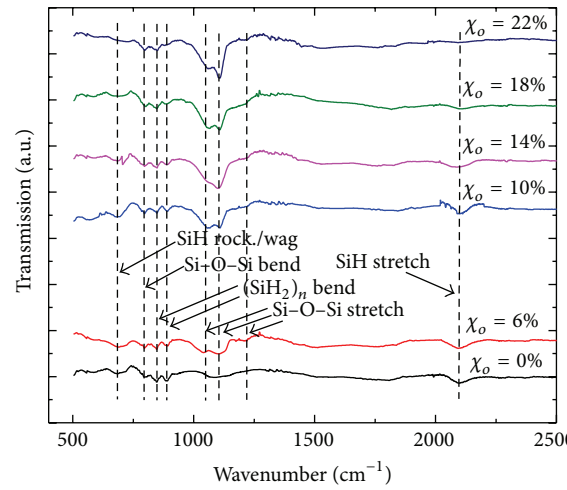

FIGURE 4: FTIR transmission spectra of a-SiO$_x$:H(i) films under different χ_o. Higher O content in the film is observed with increasing CO_2 partial pressure, with Si–H(SiO$_2$) being the dominant bonding configuration. C_H increases with O content at first due to O facilitated inclusion but reduces beyond the optimal χ_o due to O induced effusion. Doublet at 845 cm^{-1} and 890 cm^{-1} shows evidence of low temperature processing. The lines are guides for the eye.

wafer temperature in this series. However, it should be noted that only a small amount of CO_2 is needed to greatly improve the passivation quality, as compared to a-Si:H(i) (denoted by 0% partial pressure in the same figure). It is also interesting to notice that the optimal CO_2 partial pressure in our ICP system is only about half of what was reported by Mueller et al. [16, 18, 20]. The difference could be a strong indication of different plasma chemistry and reactor design. The initial improvement of lifetime with respect to CO_2 flow rate can be explained by the increase of H content (C_H) in the film. Higher CO_2 partial pressure in the plasma induces higher O content inside the resultant film. As H atoms can easily bond to Si atoms that are back bonded by O atoms [49], higher C_H is expected due to O incorporation. Indeed, this argument will be supported with FTIR spectra and H content calculations.

Once beyond the optimal point, lifetime starts to reduce with increasing CO_2 flow rate. Several groups [16, 18, 19] attribute this phenomenon to increasing defect density due to higher C impurity concentration in the film. Considering similar CO_2 partial pressure used by Mueller et al. [16, 18] and Hoex et al. [19] compared to this work, higher impurity incorporation can be regarded as one of the reasons that cause lifetime degradation at higher CO_2 flow rate in this study as well. However, by examining FTIR spectra and bonding configuration under different CO_2 flow conditions, it can be concluded that the reduction of C_H at higher O concentration is a key reason for the degradation beyond the optimal point. TOF SIMS analysis also reveals that the concentration of C atoms in a-SiO$_x$:H(i) is quite small even at the highest χ_o used in this work.

3.2.2. Bonding Configuration Analysis. In order to further investigate the influence of CO_2 partial pressure on the film property, FTIR analysis was carried out. The results are shown in Figure 4. Note that for all samples, contribution from O–H bonding group is not observable, which is similar to other a-SiO$_x$:H(i) thin films commonly reported in the literature [15, 19, 37]. The Si–C or C–H bonding configuration is also not clearly visible in the spectra due to extremely small inclusion of C atoms in the film [50, 51].

From Figure 4, it can be observed that Si–O–Si stretching peak intensity increases with χ_o. The observed small peak for spectrum with 0 sccm CO_2 flow is probably due to thin native oxide grown on the wafer during transfer. Assuming the peak intensity is proportional to O concentration in the film [38, 52], it can be concluded that the film contains higher O content with increasing CO_2 flow. It is interesting to observe that the Si–O–Si stretching peak at 1107 cm^{-1} becomes more significant with higher χ_o compared to that at 1053 cm^{-1}. Jana et al. [37] and Zhou et al. [15] associate these peaks to Si–H(Si$_{3-n}$O$_n$) with $n = 2$ and 1, respectively, according to random bonding model [53]. The increase of peak intensity at 1107 cm^{-1} indicates an increase of Si–H(SiO$_2$) bonding concentration. The shift of overall Si–O–Si stretching mode to a higher wavenumber is also an indication of higher O content in the film [54, 55]. Therefore, high O content and higher order Si–O–Si bonding configuration resulted in high CO_2 flow condition. The highest O bonding configuration at 1156 cm^{-1} reported by the mentioned groups is not clearly observed even at over 20% CO_2 partial pressure in our case, indicating that Si–H(SiO$_2$) is the dominant bonding configuration in the χ_o range used in this paper. Notably, two sharp peaks appear at 845 cm^{-1} and 890 cm^{-1}, which are not commonly observed in a-SiO$_x$:H(i) spectra. This doublet is associated with the polymer chain, (SiH$_2$)$_n$, in the film. The appearance of such a doublet is an indicator for low process temperature [38]. Therefore, the lifetime result in this section is much lower than optimized.

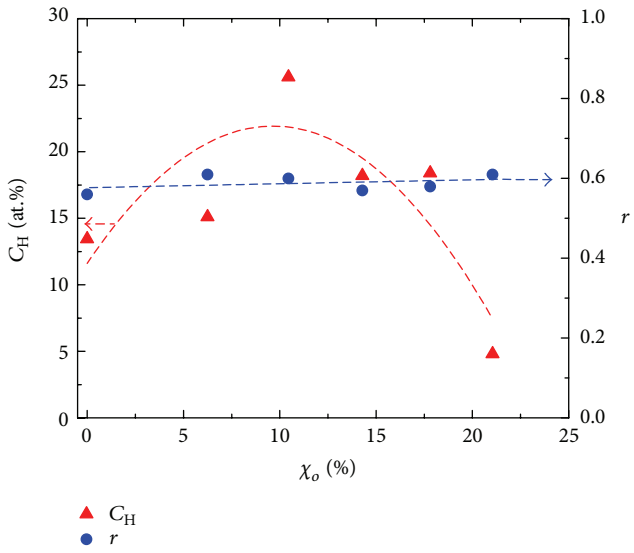

FIGURE 5: C_H and r as functions of χ_o. C_H displays a peak at about 10% CO_2 partial pressure, while r is insensitive to χ_o variation. The lines are guides for the eye.

The peaks at 640 cm^{-1} and 2000 cm^{-1} denote Si–H rocking/wagging and stretching mode [35], respectively. Total H content and bonding configuration can be deduced from these peaks [56]. The results are shown in Figure 5.

It can be observed that C_H inside the film increases with χ_o. Compared with Figure 4, the increase of C_H can be regarded as the result of increasing O content in the film at higher CO_2 flow rate. At the same time, increasing O incorporation does not significantly affect the microstructure factor. Therefore, the improvement of passivation quality is mainly due to the increasing amount of H atoms that can saturate the interface dangling bonds. Indeed, when O content is further increased beyond the optimal point, C_H starts to decrease, leading to a reduction of τ_{eff}. The reduction of C_H could be due to the increased H effusion rate at low temperature as a function of O content in the film. The O cluster formed at higher χ_o induces a void-rich network and promotes the effusion of H atoms [57, 58]. Same fluctuation and reduction of H content with increasing O content was also observed by Janotta et al. [49]and Yun et al. [52]. The direct dependence of passivation quality on C_H indicates that besides impurity incorporation, C_H in a-SiO_x:H(i) still dominates the passivation quality, which can be adjusted by χ_o. The same dependence on C_H is also widely observed in a-Si:H(i) [10]. However, higher passivation quality of a-SiO_x:H(i) comes from the fact that it has much higher C_H (>20 at.% in our case) compared to that in a-Si:H(i) (12–14 at.%) [16, 59].

3.2.3. Film Composition Analysis. In order to get more insight on the elemental composition of a-SiO_x:H(i) films deposited at various χ_o, TOF SIMS analysis was carried out to quantify the depth-resolved concentration for C and O. The results are shown in Figure 6.

Similar to the result obtained by FTIR, O concentration increases with CO_2 partial pressure (cf. Figure 6(a)). The highest O concentration achieved in this work is about 7 × 10^{20} cm^{-3}, which agrees well with Mueller et al. [16] at a similar CO_2 partial pressure. It should be noted that the uneven distribution of O content throughout the film could be related to the specific depth resolution of SIMS technique used in this paper. The thinness of the film and short deposition duration could also cause such an observation.

Figure 6(b) shows the change of C impurity concentration in the passivation film at different χ_o. C concentration increases at about one order of magnitude for a CO_2 partial pressure change of 20%. C content in this study is slightly higher compared to the result obtained by Mueller et al. [16]. This could be due to the difference in plasma chemistry and reactor design. Nevertheless, the highest C content in the film is only about 0.1 at.%, and it is not sensitive to the change in CO_2 partial pressure. Therefore, the change of H content in the film is the main reason for the change of passivation quality, as concluded in the previous sections.

3.3. Process Temperature

3.3.1. Passivation Quality. In Section 3.2.2, we have shown that the used process temperature is below optimum. Therefore, a scan in process temperature while fixing film thickness at 20 nm and χ_o (10%) at optimum was performed. Other plasma parameters were kept constant. The result for temperature dependent passivation quality is shown in Figure 7.

The temperature process window of a-SiO_x:H(i) in ICP system seems to be very wide compared to a-Si:H(i) thin film [12]. For a very broad temperature range (over 200°C), the lifetime stays above 1 ms, demonstrating a very stable process with suppression of epitaxial formation by a-SiO_x:H(i) thin film [15, 60]. Despite the stable lifetime, a peak is apparently present near 250–300°C, with a lifetime exceeding 4 ms at about 300°C. The excellent passivation quality is mainly due to a very high H content at the optimal condition.

The initial increase of lifetime is due to better bonding structure benefited from thermal relaxation [42, 61]. Higher temperature releases incorporated H atoms from trapped state (Si–H_2), which is reflected by a reducing r (see Figure 9). These H atoms are mobilized to saturate the interface dangling bonds, thus providing chemical passivation. This phenomenon is further investigated in the following section using FTIR. Once beyond the optimal temperature, the lifetime reduces as a result of H effusion. Indeed, 300°C seems to be the optimal process temperature in our ICP system, which agrees with H effusion temperature reported in the literature [16, 62]. The slightly lower effusion temperature is probably due to the difference in material and deposition technique. The reduction in C_H is the cause of deteriorated passivation quality due to insufficient interface dangling bond saturation.

3.3.2. Bonding Configuration Analysis. In order to understand the temperature dependence of a-SiO_x:H(i) passivation, FTIR analysis was carried out. The main features on

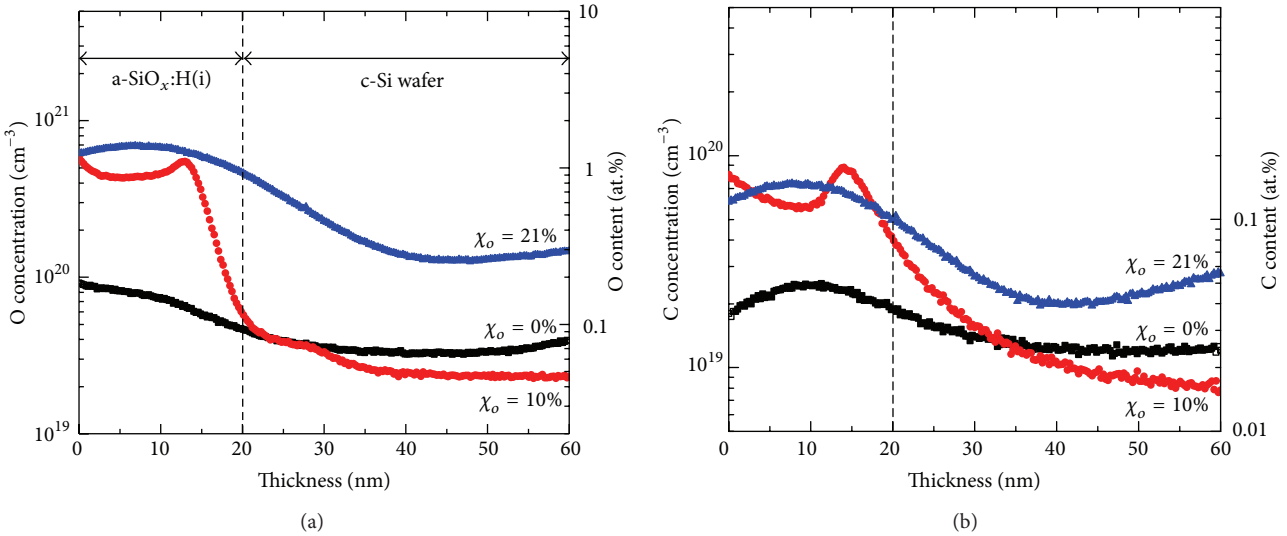

FIGURE 6: Depth resolved (a) O and (b) C concentrations obtained from TOF SIMS. The respective elemental content in a-Si host is calculated based on standard c-Si atomic concentration. Both O and C concentrations show increasing trend with respect to CO_2 partial pressure during deposition. The highest C content achievable in this work is about 0.1 at.%.

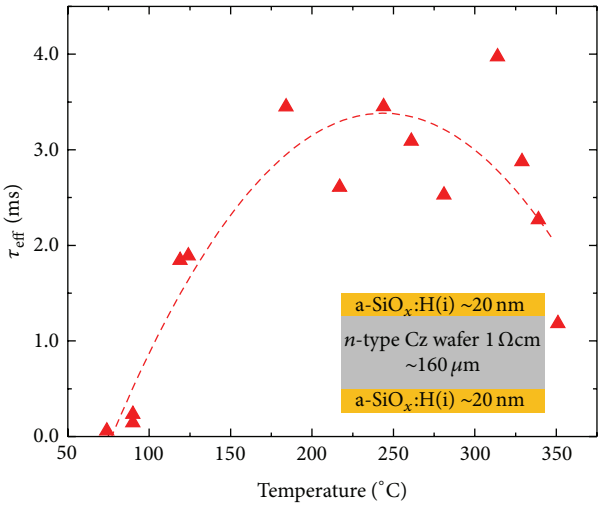

FIGURE 7: Effective lifetime as a function of process temperature. A relatively large process window is observed, which makes the a-SiO$_x$:H films less sensitive to deposition temperature. The line is a guide to the eye. The inset shows the sample structure for lifetime extraction.

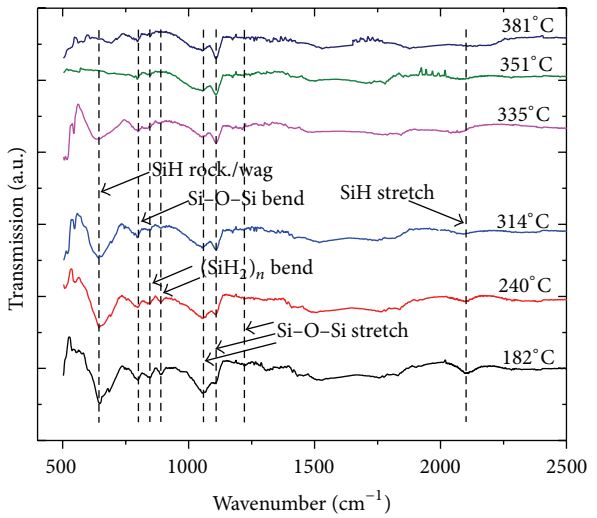

FIGURE 8: FTIR transmission spectra of a-SiO$_x$:H(i) films with different process temperatures. O in the film tends to be bonded in higher order configuration with increasing temperature. The diminishing peak at 640 cm^{-1} and 2000 cm^{-1} indicates the effusion of H atoms. The disappearance of doublet at 845 cm^{-1} and 890 cm^{-1} indicates the optimised temperature. The lines are guide to the eye.

FTIR transmission spectra are similar to those shown in Figure 4. The results are illustrated in Figure 8.

The intensity change in Si–O–Si stretching mode peaks with respect to process temperature is not evident, indicating a roughly constant O content in the film throughout the temperature range used. This is reasonable as χ_o is kept constant in this section. However, the shift of O bonding structure to higher order (Si–H(SiO$_2$)) with temperature is more prominent in this temperature series compared to the previous sections, as evidenced from the heightening and sharpening of the peak at 1107 cm^{-1}. It seems that process temperature and χ_o has similar effect in altering the bonding configuration inside the film. The shift of Si–O–Si stretching peak position at high temperature is also observed by Yun et al. [52] and is caused by the disproportionation of the reaction chemistry of a-SiO$_x$:H(i) into a more oxygen-rich suboxide.

In order to find the direct reason for improved lifetime with respect to temperature, C_H and r are calculated following the same procedure described in Section 3.2.2. The results are illustrated in Figure 9.

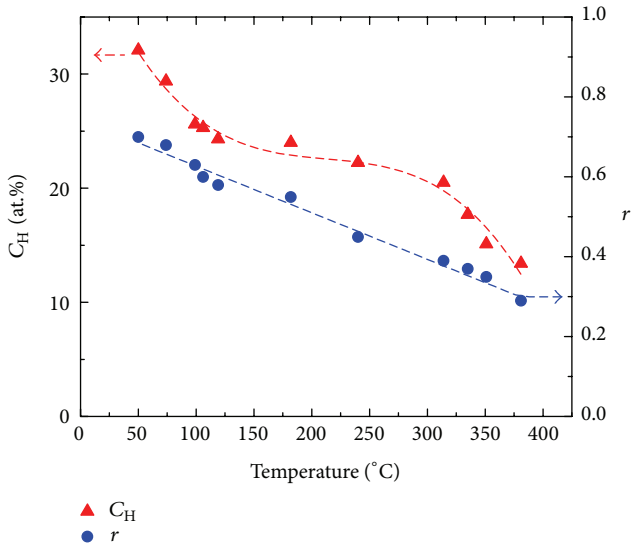

Figure 9: C_H and r as functions of temperature. The C_H displays a gradual reduction with a plain over a large span of temperature, resulting in good lifetime with a wide process window. The lines are guides for the eye.

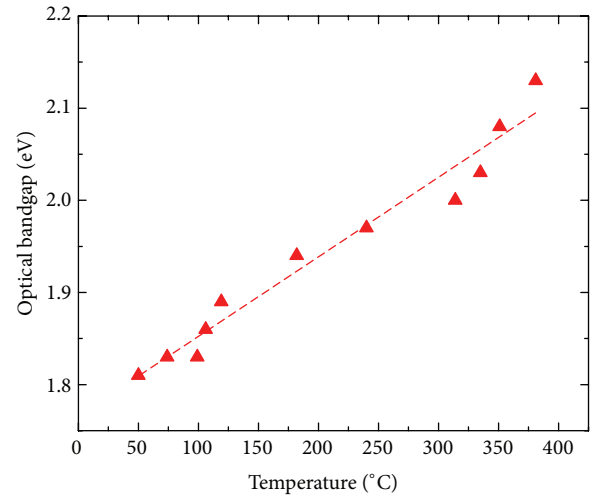

Figure 10: Optical bandgap as a function of process temperature. The line is a guide for the eye. A linear dependence of bandgap on temperature can be observed.

C_H at low temperature is over 30 at.%, indicating a void-rich network with a dominating $Si–H_2$ bonding configuration. The defective network is also evident from strong $(SiH_2)_n$ doublet peaks at 845 cm^{-1} and 890 cm^{-1}, similar to those observed in Figure 4. With increasing temperature, C_H reduces in a nonlinear behaviour, showing a plain over a wide range of temperature. At the same time, the intensity of the doublet reduces, indicating a better network structure at elevated temperature. On the other hand, r reduces in a linear manner, indicating a better a-SiO_x:H(i) network with less H clusters and microvoids [42, 61]. The combination of a high C_H due to slow H depletion and an improved amorphous network results in an excellent passivation quality within the process window observed in Figure 7. It is interesting to notice that the sudden reduction of lifetime in Figure 6 coincides with the abrupt loss of H in Figure 9 at around 300°C. As 300°C is close to the commonly reported temperature at which H effusion takes place, the reduction of lifetime beyond the optimal temperature is indeed due to H effusion. Comparing the trend shown in Figures 7 and 9, it can be concluded that the passivation quality of a-SiO_x:H(i) is strongly influenced by C_H in the film, similar to its a-Si:H(i) counterpart. This observation is also intuitive because interface passivation in such samples utilizes H atoms to saturate the dangling bonds as well. Yet, in this study, the apparent large process window in terms of temperature is mainly benefited from the gentle and wide slope that crosses a temperature range of more than 200°C, with a constantly decreasing r. The excellent lifetime at optimal condition is a result of much higher C_H (over 20 at.%) compared to standard a-Si:H(i) thin film [59], as mentioned in Section 3.2.2.

It should be noted that several groups [63, 64] reported improved lifetimes after an H plasma postdeposition treatment with even increasing r. This seems contradictory to our finding but can be attributed to greatly increased C_H upon plasma treatment, which diffuses into the interface upon annealing. The improvement of lifetime then cannot be solely explained by the bonding configuration in the amorphous structure. Indeed, the combination of both high C_H and low r in our a-SiO_x:H(i) is the key to such an excellent surface passivation quality, as concluded in the earlier discussion. In case of a-SiO_x:H(i), the use of H plasma treatment is therefore not necessary to achieve high passivation quality due to the inherent high H inclusion of the film.

3.3.3. Optical Property. The optimized a-SiO_x:H(i) has demonstrated excellent passivation properties due to enhanced H content and bonding structure. However, in order to apply the film to HET solar cells, optical properties are equally important. Therefore, Tauc's method [41] was used to find the optical bandgap from SE fitting result. The results are shown in Figure 10.

The optical bandgap increases almost linearly with deposition temperature despite the fact that C_H reduces, as shown in Figure 9. In the case of a-Si:H(i), optical bandgap is positively dependent on C_H in the film [65]. In our case, the contradiction could possibly be explained with an altered O bonding structure. As shown in Figure 8, the elevated temperature shifts the O bonding configuration in a-SiO_x:H(i) thin films to a higher mode and could possibly cause an increase in the stoichiometry parameter x in the a-SiO_x:H(i) film. This change can be one of the reasons for the improved optical bandgap. The optical bandgap at optimal temperature is above 2 eV, which greatly suppresses optical absorption at low wavelengths and improves J_{sc} when applied in HET solar cells.

On the other hand, the film thickness reduces slightly (not shown) with process temperature despite the same deposition time. Since the thickness is obtained from SE fitting, one can argue that the reduction of thickness is due to increased

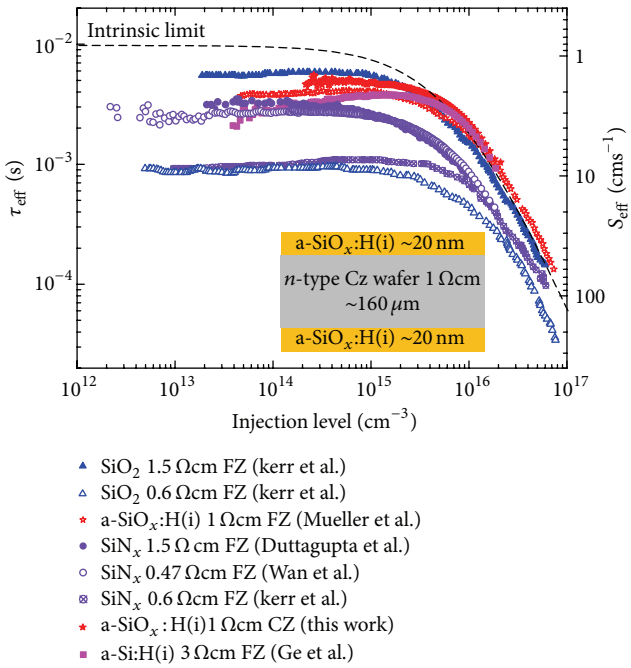

FIGURE 11: Measured QSSPC lifetime of optimized a-SiO$_x$:H(i) film as a function of minority carrier injection level. The calculation of effective surface recombination velocity is based on wafer thickness of our samples. The dashed line represents intrinsic limit of the 1 Ωcm wafer assuming no extrinsic recombination [27]. As a comparison, other high-quality passivation schemes from Mark and Andres [28, 29], Duttagupta et al. [30], Wan et al. [31], Mueller et al. [16, 18], and Ge et al. [10] are also shown in the graph. The inset shows the sample structure for ICP a-SiO$_x$:H(i) passivation.

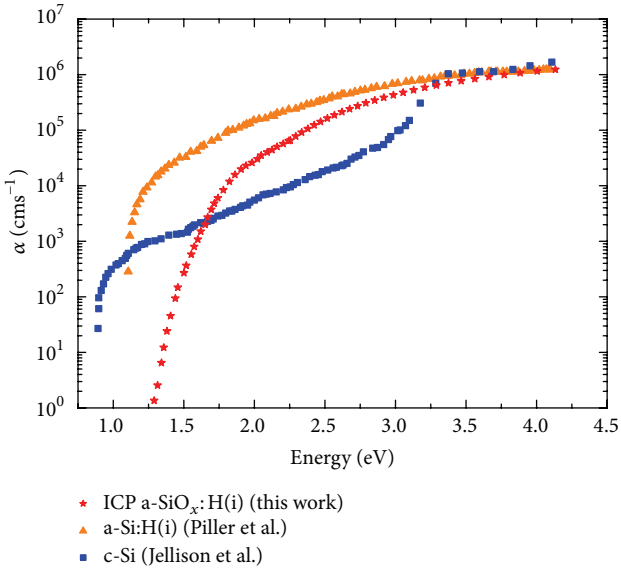

FIGURE 12: Absorption coefficient as a function of photon energy. For comparison, the absorption coefficients of crystalline Si (Jellison 3-1-91) [32] and a-Si:H(i) [33] are shown in the same graph. ICP a-SiO$_x$:H(i) film shows excellent optical properties compared to a-Si:H(i) throughout the whole wavelength range.

film density at higher temperature. Indeed, the loss of H content and the reduction of microvoid volume (see Figure 9) indicate an optically compact network, therefore causing a reduction in the film thickness. The reduction of thickness also has an impact on the film morphology, altering its crystallinity and optical bandgap as well [66].

3.4. Comparison with Existing Passivation Schemes

3.4.1. Passivation Quality. In order to demonstrate the excellent surface passivation result of the optimized a-SiO$_x$:H(i) thin film, a comparison in terms of lifetime between our film and some other high-quality passivation schemes was made. The result is shown in Figure 11. By assuming identical surface passivation on both sides of the wafer and sufficiently low surface recombination, the effective surface recombination velocity (S_{eff}) can be related to τ_{eff} using the following relationship:

$$S_{eff} = \frac{W}{2}\left(\frac{1}{\tau_{eff}} - \frac{1}{\tau_{bulk}}\right), \quad (3)$$

where W is the thickness of the wafer and τ_{bulk} represents the bulk lifetime of the wafer, which is a combined result of Auger, radiative, and Shockley-Read-Hall recombination. By further assuming a perfect bulk quality (i.e., $\tau_{bulk} \to \infty$), the upper limit of S_{eff} can be calculated using (3). From the same equation, it can be shown that the lower the S_{eff}, the better the surface passivation quality.

From Figure 11 it can be concluded that the a-SiO$_x$:H(i) thin film reported in this paper has similar high-quality passivation quality compared to other schemes, despite the usage of Cz wafers in this work. It should be noted that the reported lifetimes in this work are as-deposited values. Comparing the passivation quality of the a-SiO$_x$:H(i) film in this work to that of Mueller et al. [16, 18], which appears to be the record lifetime on low-resistivity wafers at the time of reporting, the ICP a-SiO$_x$:H(i) films deposited in this work yield a slightly better passivation quality which may be attributed to the lower damage remote ICP deposition. The optimized a-SiO$_x$:H(i) passivation layer features a very high lifetime of over 4.7 ms at an injection level of 10^{15} cm^{-3} with an equivalent S_{eff} of below 1.7 cms^{-1} and an implied V_{oc} of 741 mV. This passivation quality is excellent considering the wafer type that was used. Therefore, the ICP a-SiO$_x$:H(i) has demonstrated great potential to be used in HET solar cells.

3.4.2. Optical Properties. As a passivation layer in HET solar cells, the layer should not only have excellent electronic passivation quality but also be highly transparent so as to reduce optical absorption in the layer. The better optical property also allows the use of slightly thicker passivation layer to enhance the passivation quality. Therefore, material with high bandgap with low absorption coefficient is preferred.

We have demonstrated excellent passivation quality of our ICP a-SiO$_x$:H(i) thin film in the previous section. An ideal bandgap of about 2 eV is also illustrated. A comparison of α of our film and other materials is made in Figure 12.

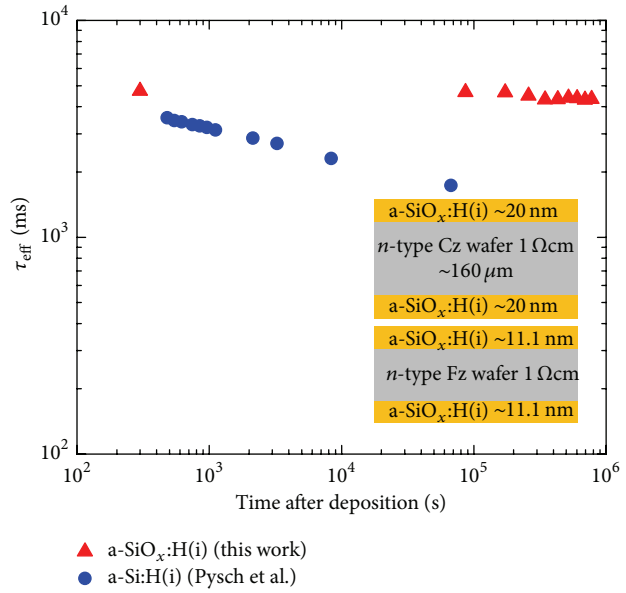

Figure 13: Effective lifetime as a function of time after deposition. The insets show sample structures and dimensions for both materials used in the degradation study. The passivation quality of a-SiO$_x$:H(i) film (20 nm) hardly degrades even after one week of storage. As a comparison, lifetime degradation data of ICP a-Si:H(i) [24] (11.1 nm) is superposed in the same graph. The a-Si:H(i) passivation layer shows constant degradation of lifetime immediately after deposition.

Comparing to the standard a-Si:H(i) film, ICP a-SiO$_x$:H(i) has much lower α across the whole energy range in Figure 12, showing excellent optical property. This might be due to suppressed band-to-band absorption and subband absorption, benefiting from the high bandgap and the low defect density in the film. Therefore, the ICP a-SiO$_x$:H(i) deposited in this work has superior optical properties.

3.4.3. Stability. In this section, we investigate the stability of the passivation layer by storing the samples in dark environment and monitoring the passivation quality of the films in regular intervals. The first lifetime measurement was usually conducted two minutes after deposition of the film. The subsequent measurements were made once every 24 hours, throughout a period of one week. The results are shown in Figure 13.

It can be observed that the ICP a-SiO$_x$:H(i) film (20 nm) in the as-deposited state shows negligible degradation after one week of storage, as reflected by the almost constant τ_{eff} over time. On the other hand, the ICP a-Si:H(i) from Pysch et al. shows severe degradation after two days of storage. The relatively more stable behaviour of ICP a-SiO$_x$:H(i) might be due to (a) slightly thicker film in this work that shields the delicate interface from the environment and (b) a less sensitive interface against degradation due to the incorporation of O atoms during deposition. Therefore, it can be concluded that the passivation film developed in the present work is robust against degradation caused by exposure to the ambient environment. It should be noted that passivated wafers are usually sent for subsequent processing (doped layers and TCO depositions) immediately after deposition. Long-time exposure to the ambient environment is rarely observed in industrial processes. Thus, the stable ICP a-SiO$_x$:H(i) will definitely maintain its excellent passivation quality during the short time periods between the different processes. The same stable behaviour is also reported by Larionova et al. [67], however, only with a SiN$_x$ capping layer.

4. Conclusion

In this paper, we presented a novel passivation scheme featuring low-temperature ICPECVD a-SiO$_x$:H(i) thin films. By tuning the CO_2 partial pressure and process temperature, the thin film was optimized in terms of passivation and optical quality. An excellent as-deposited lifetime on solar-grade highly doped *n*-type Cz wafers of over 4.7 ms with S_{eff} less than 1.7 cm s^{-1} was obtained. At the same time, the film also had high bandgap and low absorption, showing excellent optical properties as well. Comparing to typically used a-Si:H(i), the ICP a-SiO$_x$:H(i) shows superior stability against degradation after being exposed to ambient environment. We propose the ICP a-SiO$_x$:H(i) as an alternative candidate for high-quality surface passivation layers in HET solar cell applications.

Conflict of Interests

The authors declare that there is no conflict of interests regarding the publication of this paper.

Acknowledgments

The Solar Energy Research Institute of Singapore is sponsored by the National University of Singapore (NUS) and Singapore's National Research Foundation (NRF) through the Singapore Economic Development Board (EDB). This research is supported by the National Research Foundation, Prime Minister's Office, Singapore under its Clean Energy Research Programme (CERP Award no. NRF2010EWT-CERP001-022).

References

[1] M. Taguchi, A. Yano, S. Tohoda et al., "24.7% record efficiency HIT solar cellon thin silicon wafer," *IEEE Journal of Photovoltaics*, vol. 99, pp. 1–4, 2013.

[2] M. Taguchi, Y. Tsunomura, H. Inoue et al., "High-efficiency HIT solar cell on thin (<100 μm) silicon wafer," in *Proceedings of the 24th European Photovoltaic Solar Energy Conference*, pp. 1690–1693, 2009.

[3] Y. Tsunomura, Y. Yoshimine, M. Taguchi et al., "Twenty-two percent efficiency HIT solar cell," *Solar Energy Materials and Solar Cells*, vol. 93, no. 6-7, pp. 670–673, 2009.

[4] J.-W. A. Schttauf, K. H. M. van der Werf, I. M. Kielen, W. G. J. H. M. van Sark, J. K. Rath, and R. E. I. Schropp, "High quality crystalline silicon surface passivation by combined intrinsic and *n*-type hydrogenated amorphous silicon," *Applied Physics Letters*, vol. 99, no. 20, Article ID 203503, 2011.

[5] M. Taguchi, K. Kawamoto, S. Tsuge et al., "HIT ells-high-efficiency crystalline Si cells with novel structure," *Progress in Photovoltaics: Research and Applications*, vol. 8, pp. 503–513, 2000.

[6] M. Tanaka, M. Taguchi, T. Matsuyama et al., "Development of new a-Si/c-Si heterojunction solar cells: ACJ-HIT (Artificially Constructed Junction-Heterojunction with Intrinsic Thin-layer)," *Japanese Journal of Applied Physics*, vol. 31, no. 11, pp. 3518–3522, 1992.

[7] J. I. Pankove and M. L. Tarng, "Amorphous silicon as a passivant for crystalline silicon," *Applied Physics Letters*, vol. 34, no. 2, pp. 156–157, 1979.

[8] M. Taguchi, A. Terakawa, E. Maruyama, and M. Tanaka, "Obtaining a higher voc in HIT cells," *Progress in Photovoltaics: Research and Applications*, vol. 13, no. 6, pp. 481–488, 2005.

[9] K. Wakisaka, M. Taguchi, T. Sawada et al., "More than 16% solar cells with a new "HIT" (doped a-Si/non-doped a-Si/crystalline Si) structure," in *Proceedings of the IEEE Photovoltaic Specialists Conference*, pp. 887–892, October 1991.

[10] J. Ge, Z. P. Ling, J. Wong, T. Mueller, and A. G. Aberle, "Optimisation of Intrinsic a-Si:H passivation layers in crystalline-amorphous silicon heterojunction solar cells," *Energy Procedia*, vol. 15, pp. 107–117, 2012.

[11] J. Ge, Z. P. Ling, J. Wong, R. Stangl, A. G. Aberle, and T. Mueller, "Analysis of intrinsic hydrogenated amorphous silicon passivation layer growth for use in heterojunction silicon wafer solar cells by optical emission spectroscopy," *Journal of Applied Physics*, vol. 113, no. 23, Article ID 234310, 2013.

[12] H. Fujiwara and M. Kondo, "Impact of epitaxial growth at the heterointerface of solar cells," *Applied Physics Letters*, vol. 90, Article ID 013503, 2007.

[13] U. Kroll, J. Meier, P. Torres, J. Pohl, and A. Shah, "From amorphous to microcrystalline silicon films prepared by hydrogen dilution using the VHF (70 MHz) GD technique," *Journal of Non-Crystalline Solids*, vol. 227–230, part 1, pp. 68–72, 1998.

[14] S. de Wolf and M. Kondo, "Abruptness of interface revealed by carrier lifetime measurements," *Applied Physics Letters*, vol. 90, Article ID 042111, 2007.

[15] H. P. Zhou, D. Y. Wei, S. Xu et al., "Si surface passivation by SiO_x : H films deposited by a low-frequency ICP for solar cell applications," *Journal of Physics D: Applied Physics*, vol. 45, Article ID 395401, 2012.

[16] T. Mueller, S. Schwertheim, and W. R. Fahrner, "Crystalline silicon surface passivation by high-frequency plasma-enhanced chemical-vapor-deposited nanocomposite silicon suboxides for solar cell applications," *Journal of Applied Physics*, vol. 107, no. 1, Article ID 014504, 2010.

[17] G.-Z. Jia, H.-G. Liu, and H.-D. Chang, "PECVD amorphous silicon suboxide films for surface passivation of silicon solar cells," in *Proceedings of the 10th IEEE International Conference on Solid-State and Integrated Circuit Technology*, pp. 2013–2015, November 2010.

[18] T. Mueller, S. Schwertheim, M. Scherff, and W. R. Fahrner, "High quality passivation for heterojunction solar cells by hydrogenated amorphous silicon suboxide films," *Applied Physics Letters*, vol. 92, no. 3, Article ID 033504, 2008.

[19] B. Hoex, F. J. J. Peeters, M. Creatore, M. A. Blauw, W. M. M. Kessels, and M. C. M. van de Sanden, "High-rate plasma-deposited SiO_2 films for surface passivation of crystalline silicon," *Journal of Vacuum Science and Technology A: Vacuum, Surfaces and Films*, vol. 24, no. 5, pp. 1823–1830, 2006.

[20] S. Schwertheim, M. Scherff, T. Mueller, W. R. Fahrner, and H. C. Neitzert, "Lead-free electrical conductive adhesives for solar cell interconnectors," in *Proceedings of the 33rd IEEE Photovoltaic Specialists Conference, PVSC 2008*, pp. 1–6, May 2008.

[21] T. Mueller, W. Duengen, R. Job, M. Scherff, and W. Fahrner, "Crystalline silicon surface passivation by PECV-deposited hydrogenated amorphous silicon oxide films [a-SiO_x:H]," in *MRS Online Proceedings Library*, vol. 989, pp. 75–80, April 2007.

[22] S. Q. Xiao, S. Xu, H. P. Zhou et al., "Amorphous/crystalline silicon heterojunction solar cells via remote inductively coupled plasma processing," *Applied Physics Letters*, vol. 100, no. 23, Article ID 233902, 2012.

[23] J. Li, J. Wang, M. Yin et al., " Deposition of controllable preferred orientation silicon films on glass by inductively coupled plasma chemical vapor deposition," *Journal of Applied Physics*, vol. 103, Article ID 043505, 2008.

[24] D. Pysch, M. Bivour, K. Zimmermann, C. Schetter, M. Hermle, and S. W. Glunz, "Comprehensive study of different PECVD deposition methods for deposition of thin intrinsic amorphous silicon for heterojunction solar cells," in *Proceedings of the 24th European Photovoltaic Solar Energy Conference*, pp. 1580–1585, 2009.

[25] Z. Zhang, T. Dippell, M. Huber et al., "SINGULAR platform for dual-sided plasma treatment and coating of Si-based passivation layers," in *Proceedings of the 29th European Photovoltaic Solar Energy Conference*, 2014.

[26] J. Ge, M. Tang, J. Wong et al., "State-of-the-art amorphous silicon sub-oxide passivation layer by ICPECVD for heterojunction solar cell applications," in *Proceedings of the 29th European Photovoltaic Solar Energy Conference*, 2014.

[27] A. Richter, F. Werner, A. Cuevas, J. Schmidt, and S. W. Glunz, "Improved parameterization of auger recombination in silicon," *Energy Procedia*, vol. 27, pp. 88–94, 2012.

[28] J. K. Mark and C. Andres, "Very low bulk and surface recombination in oxidized silicon wafers," *Semiconductor Science and Technology*, vol. 17, p. 35, 2002.

[29] J. K. Mark and C. Andres, "Recombination at the interface between silicon and stoichiometric plasma silicon nitride," *Semiconductor Science and Technology*, vol. 17, p. 166, 2002.

[30] S. Duttagupta, F. Lin, M. Wilson, M. B. Boreland, B. Hoex, and A. G. Aberle, "Extremely low surface recombination velocities on low-resistivity *n*-type and *p*-type crystalline silicon using dynamically deposited remote plasma silicon nitride films," *Progress in Photovoltaics: Research and Applications*, vol. 22, no. 6, pp. 641–647, 2012.

[31] Y. Wan, K. R. McIntosh, A. F. Thomson, and A. Cuevas, "Low surface recombination velocity by low-absorption silicon nitride on c-Si," *IEEE Journal of Photovoltaics*, vol. 3, no. 1, pp. 554–559, 2013.

[32] G. E. Jellison Jr., "Optical functions of GaAs, GaP, and Ge determined by two-channel polarization modulation ellipsometry," *Optical Materials*, vol. 1, no. 3, pp. 151–160, 1992.

[33] H. Piller, *Handbook of Optical Constants of Solids*, vol. 1, 1985.

[34] C. T. Kirk, "Quantitative analysis of the effect of disorder-induced mode coupling on infrared absorption in silica," *Physical Review B*, vol. 38, pp. 1255–1273, 1988.

[35] L. He, Y. Kurata, T. Inokuma, and S. Hasegawa, "Analysis of SiH vibrational absorption in amorphous SiO_x:H ($0 \le x \le 2.0$) alloys in terms of a charge-transfer model," *Applied Physics Letters*, vol. 63, no. 2, pp. 162–164, 1993.

[36] M. H. Brodsky, M. Cardona, and J. J. Cuomo, "Infrared and Raman spectra of the silicon-hydrogen bonds in amorphous silicon prepared by glow discharge and sputtering," *Physical Review B*, vol. 16, no. 8, pp. 3556–3571, 1977.

[37] T. Jana, S. Mukhopadhyay, and S. Ray, "Low temperature silicon oxide and nitride for surface passivation of silicon solar cells," *Solar Energy Materials and Solar Cells*, vol. 71, no. 2, pp. 197–211, 2002.

[38] G. Lucovsky, J. Yang, S. S. Chao, J. E. Tyler, and W. Czubatyj, "Oxygen-bonding environments in glow-discharge-deposited amorphous silicon-hydrogen alloy films," *Physical Review B*, vol. 28, no. 6, pp. 3225–3233, 1983.

[39] H. Nagel, C. Berge, and A. G. Aberle, "Generalized analysis of quasi-steady-state and quasi-transient measurements of carrier lifetimes in semiconductors," *Journal of Applied Physics*, vol. 86, no. 11, pp. 6218–6221, 1999.

[40] G. E. Jellison Jr. and F. A. Modine, "Parameterization of the optical functions of amorphous materials in the interband region," *Applied Physics Letters*, vol. 69, no. 3, pp. 371–373, 1996.

[41] J. Tauc, "Optical properties and electronic structure of amorphous Ge and Si," *Materials Research Bulletin*, vol. 3, pp. 37–46, 1968.

[42] T. F. Schulze, H. N. Beushausen, C. Leendertz, A. Dobrich, B. Rech, and L. Korte, "Interplay of amorphous silicon disorder and hydrogen content with interface defects in amorphous/crystalline silicon heterojunctions," *Applied Physics Letters*, vol. 96, no. 25, Article ID 252102, 2010.

[43] J. K. Rath, R. E. I. Schropp, and W. Beyer, "Hydrogen at compact sites in hot-wire chemical vapour deposited polycrystalline silicon films," *Journal of Non-Crystalline Solids*, vol. 266–269, pp. 190–194, 2000.

[44] D. Gracin, U. Desnica, and M. Ivanda, "Microstructural properties of dc magnetron sputtered a-Si:H by IR spectroscopy," *Journal of Non-Crystalline Solids*, vol. 149, no. 3, pp. 257–263, 1992.

[45] A. H. M. Smets, W. M. M. Kessels, and M. C. M. van de Sanden, "Vacancies and voids in hydrogenated amorphous silicon," *Applied Physics Letters*, vol. 82, no. 10, pp. 1547–1549, 2003.

[46] Z. Remeš, M. Vaněček, A. H. Mahan, and R. S. Crandall, "Silicon network relaxation in amorphous hydrogenated silicon," *Physical Review B*, vol. 56, pp. R12710–R12713, 1997.

[47] Z. Remeš, M. Vaněček, P. Torres, U. Kroll, A. H. Mahan, and R. S. Crandall, "Optical determination of the mass density of amorphous and microcrystalline silicon layers with different hydrogen contents," *Journal of Non-Crystalline Solids*, vol. 227–230, part 2, pp. 876–879, 1998.

[48] D. Pysch, C. Meinhardt, K.-U. Ritzau et al., "Comparison of intrinsic amorphous silicon buffer layers for silicon heterojunction solar cells deposited with different PECVD techniques," in *Proceedings of the 35th IEEE Photovoltaic Specialists Conference (PVSC '10)*, pp. 3570–3576, June 2010.

[49] A. Janotta, R. Janssen, M. Schmidt et al., "Doping and its efficiency in a–SiO_x:H," *Physical Review B*, vol. 69, p. 115206, 2004.

[50] A. Grill and D. A. Neumayer, "Structure of low dielectric constant to extreme low dielectric constant SiCOH films: Fourier transform infrared spectroscopy characterization," *Journal of Applied Physics*, vol. 94, no. 10, pp. 6697–6707, 2003.

[51] D. M. Wolfe, B. J. Hinds, F. Wang et al., "Thermochemical stability of silicon-oxygen-carbon alloy thin films: a model system for chemical and structural relaxation at SiC-SiO_2 interfaces," *Journal of Vacuum Science and Technology A*, vol. 17, no. 4, pp. 2170–2177, 1999.

[52] F. Yun, B. J. Hinds, S. Hatatani, S. Oda, Q. X. Zhao, and M. Willander, "Study of structural and optical properties of nanocrystalline silicon embedded in SiO_2," *Thin Solid Films*, vol. 375, no. 1-2, pp. 137–141, 2000.

[53] H. R. Philipp, "Optical and bonding model for non-crystalline SiO_x and SiO_xNy materials," *Journal of Non-Crystalline Solids*, vol. 8–10, pp. 627–632, 1972.

[54] D. V. Tsu, G. Lucovsky, and B. N. Davidson, "Effects of the nearest neighbors and the alloy matrix on SiH stretching vibrations in the amorphous SiOr:H ($0 < r < 2$) alloy system," *Physical Review B*, vol. 40, no. 3, pp. 1795–1805, 1989.

[55] P. G. Pai, S. S. Chao, Y. Takagi, and G. Lucovsky, " Infrared spectroscopic study of SiO_x films produced by plasma enhanced chemical vapor deposition," *Journal of Vacuum Science and Technology A*, vol. 4, pp. 689–694, 1986.

[56] H. Shanks, C. J. Fang, L. Ley, M. Cardona, F. J. Desmond, and S. Kalbitzer, "Infrared spectrum and structure of hydrogenated amorphous silicon," *Physica Status Solidi B*, vol. 100, no. 1, pp. 43–56, 1980.

[57] F. Einsele, W. Beyer, and U. Rau, "Infrared spectrum and structure of hydrogenated amorphous silicon," *Journal of Applied Physics*, vol. 112, Article ID 054905, 2012.

[58] W. Beyer, "Infrared absorption and hydrogen effusion of hydrogenated amorphous silicon-oxide films," *Journal of Non-Crystalline Solids*, vol. 266–269, part 2, pp. 845–849, 2000.

[59] R. Janssen, A. Janotta, D. Dimova-Malinovska, and M. Stutzmann, "Optical and electrical properties of doped amorphous silicon suboxides," *Physical Review B*, vol. 60, no. 19, pp. 13561–13572, 1999.

[60] H. Fujiwara, T. Kaneko, and M. Kondo, "Application of hydrogenated amorphous silicon oxide layers toc-Si heterojunction solar cells," *Applied Physics Letters*, vol. 91, Article ID 133508, 2007.

[61] M. Jeon, S. Yoshiba, and K. Kamisako, "Hydrogenated amorphous silicon film as intrinsic passivation layer deposited at various temperatures using RF remote-PECVD technique," *Current Applied Physics*, vol. 10, no. 2, pp. S237–S240, 2010.

[62] M. Park, C. W. Teng, V. Sakhrani et al., "Optical characterization of wide band gap amorphous semiconductors (a-Si:C:H): effect of hydrogen dilution," *Journal of Applied Physics*, vol. 89, no. 2, pp. 1130–1137, 2001.

[63] M. Mews, T. F. Schulze, N. Mingirulli, and L. Korte, "Hydrogen plasma treatments for passivation of amorphous-crystalline silicon-heterojunctions on surfaces promoting epitaxy," *Applied Physics Letters*, vol. 102, no. 12, Article ID 122106, 2013.

[64] A. Descoeudres, L. Barraud, S. de Wolf et al., "Improved amorphous/crystalline silicon interface passivation by hydrogen plasma treatment," *Applied Physics Letters*, vol. 99, no. 12, Article ID 123506, 2011.

[65] G. D. Cody, C. R. Wronski, B. Abeles, R. B. Stephens, and B. Brooks, "Optical characterization of amorphous silicon hydride films," *Solar Cells*, vol. 2, no. 3, pp. 227–243, 1980.

[66] G. M. Ferreira, C. Chen, R. J. Koval, J. M. Pearce, C. R. Wronski, and R. W. Collins, "Optimization of protocrystalline silicon p-type layers for amorphous silicon n-i-p solar cells," *Journal of Non-Crystalline Solids*, vol. 338–340, no. 1, pp. 694–697, 2004.

[67] Y. Larionova, V. Mertens, N.-P. Harder, and R. Brendel, "Surface passivation of *n*-type Czochralski silicon substrates by thermal-SiO_2/plasma-enhanced chemical vapor deposition SiN stacks," *Applied Physics Letters*, vol. 96, no. 3, Article ID 032105, 2010.